

<https://doi.org/10.1038/s43247-024-01506-4>

Magnesium hydroxide addition reduces aqueous carbon dioxide in wastewater discharged to the ocean

Check for updates

Vassilis Kitidis¹✉, Stephen. A. Rackley², William. J. Burt², Greg. H. Rau², Samuel Fawcett³, Matthew. Taylor¹, Glen Tarran¹, E. Malcolm S. Woodward¹, Carolyn Harris¹ & Timothy Fileman³

Ocean alkalinity enhancement (OAE) reduces the concentration of dissolved carbon dioxide (CO₂) in seawater, leading to atmospheric carbon dioxide removal (CDR). Here we report laboratory experiments and a field-trial of alkalinity enhancement through addition of magnesium hydroxide to wastewater and its subsequent discharge to the coastal ocean. In wastewater, a 10% increase of average alkalinity (+0.56 mmol/kg) led to a 74% reduction in aqueous CO₂ (−0.41 mmol/kg) and pH increase of 0.4 units to 7.78 (efficiency 0.73 molCO₂/mol alkalinity). The alkalinization signal was limited to within a few metres of the ocean discharge, evident as 27.2 μatm reduction in CO₂ partial pressure and 0.017 unit pH increase, and was consistent with rapid dilution of the alkali-treated wastewater. While this proof of concept field trial did not achieve CDR due to its small scale, it demonstrated the potential of magnesium hydroxide addition to wastewater as a CDR solution.

Limiting global warming to 1.5 °C requires a drastic reduction of anthropogenic greenhouse gas emissions and further carbon dioxide removal (CDR) of 1–10 × 10⁹ t atmospheric CO₂ year^{−1} by mid-century^{1,2}. Ocean alkalinity enhancement (OAE) is one of the proposed solutions for CDR³. Dissolution of CO₂ in the ocean already takes up circa 26% of anthropogenic CO₂ from the atmosphere (2.9 ± 0.4 × 10⁹ t C year^{−1})^{4,5}. CO₂ dissolves in and reacts with water to form carbonic acid (H₂CO₃) which further dissociates to bicarbonate (HCO₃[−]) and carbonate ions (CO₃^{2−}), balanced by hydrogen cations (H⁺). In this context, ocean alkalinity can be thought of as a measure of the capacity of seawater to neutralise carbonic acid to HCO₃[−] and CO₃^{2−}, balanced by cations other than H⁺. Under steady state, these reactions establish an equilibrium between CO₂ in air and dissolved inorganic carbon in seawater (DIC; the sum of CO₂, H₂CO₃, HCO₃[−], CO₃^{2−}). At present, increasing atmospheric CO₂ is continually driving CO₂ influx to the ocean and increasing CO₂, acidity, and DIC which is largely removed from the surface and entrained in the deep ocean circulation for centuries to millennia. OAE also drives CO₂ into the ocean and increases DIC, but instead reduces acidity. This mimics and accelerates natural mineral weathering and ocean alkalization, thereby increasing the capacity of ocean CO₂ uptake and long-term storage of DIC^{6–8}. Addition of alkali to wastewater has recently been proposed as a vehicle for OAE and CDR⁹. Effluent from wastewater treatment is typically rich in biogenic CO₂, creating a water to air concentration gradient that drives efflux of CO₂ to the atmosphere. In principle, alkalinity enhancement of wastewater re-establishes the carbonate

equilibrium such that dissolved CO₂ gas (which can readily exchange with the atmosphere) is converted to dissolved bicarbonate and carbonate ions (which do not exchange with the atmosphere). Where treated wastewater is discharged to the ocean, alkalinity addition can thus result in: (1) ‘avoided emissions’ from the reduction of biogenic CO₂ emissions to the atmosphere and, if sufficient alkalinity has been added, (2) ocean CDR downstream of the wastewater discharge.

Numerical models have shown that OAE can effectively achieve CDR and reverse ocean acidification at the global or basin scale^{10–13}, but their predictions remain untested by field data¹⁴. Here, we report the results of laboratory experiments and a field trial of alkalinity enhancement in wastewater using a commercial magnesium hydroxide suspension (Mg(OH)₂; hereafter ‘MH’). We show that MH addition leads to a reduction in aqueous CO₂ concentration in the final effluent discharged into the coastal ocean.

Results

Wastewater alkalinity enhancement

A set of preliminary lab experiments were conducted with ‘final effluent’ from the Hayle wastewater treatment works (HWTW) in order to constrain the field trial dosing rate. A commercial MH suspension (53% as 2 μm solids; 98.5% of solids as Mg(OH)₂ or 522 g/L Mg(OH)₂, derived from calcined magnesite, was added to treated wastewater at different concentrations at 22 °C, preventing further air contact (‘closed system’).

¹Plymouth Marine Laboratory, Plymouth PL1 3DH, UK. ²Planetary Technologies, Dartmouth, NS, Canada. ³PML Applications Ltd., Plymouth PL1 3DH, UK.

✉e-mail: vak@pml.ac.uk

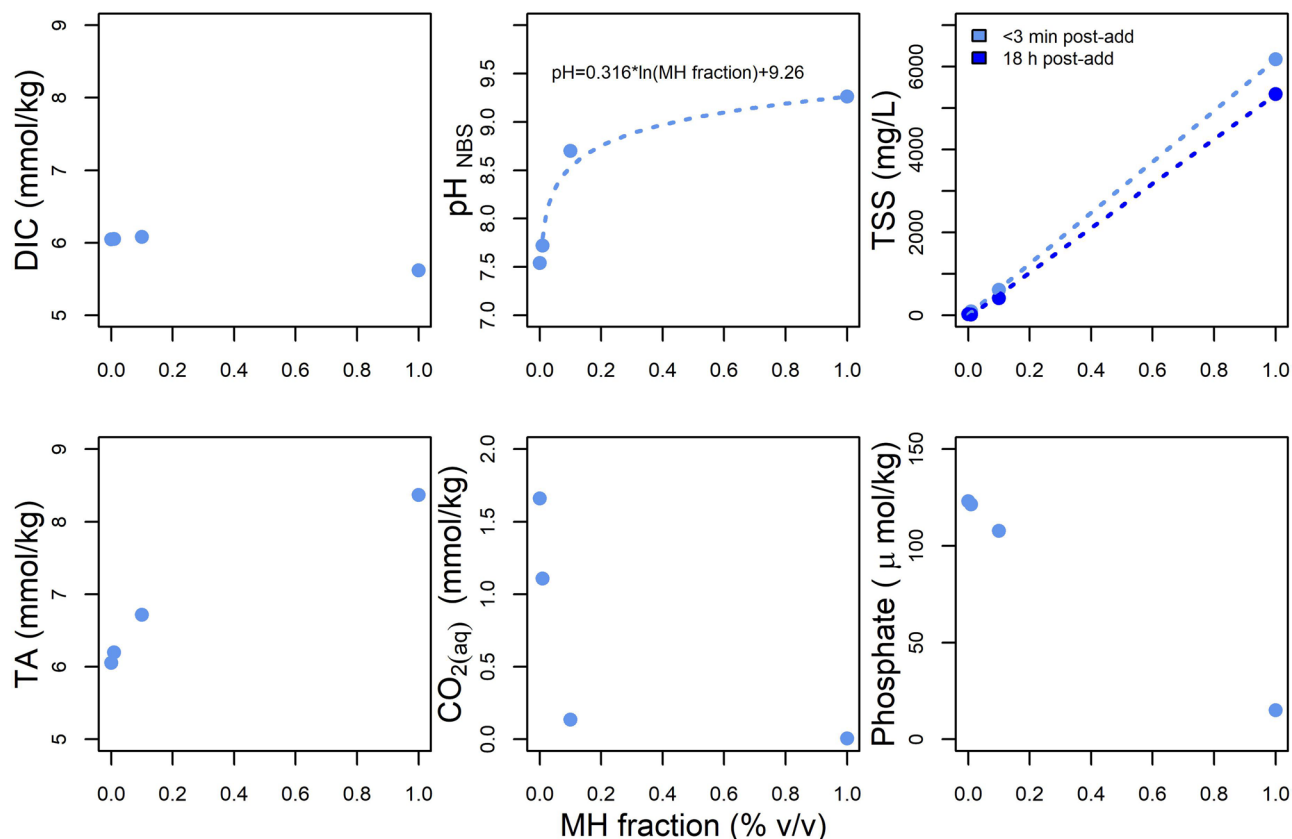


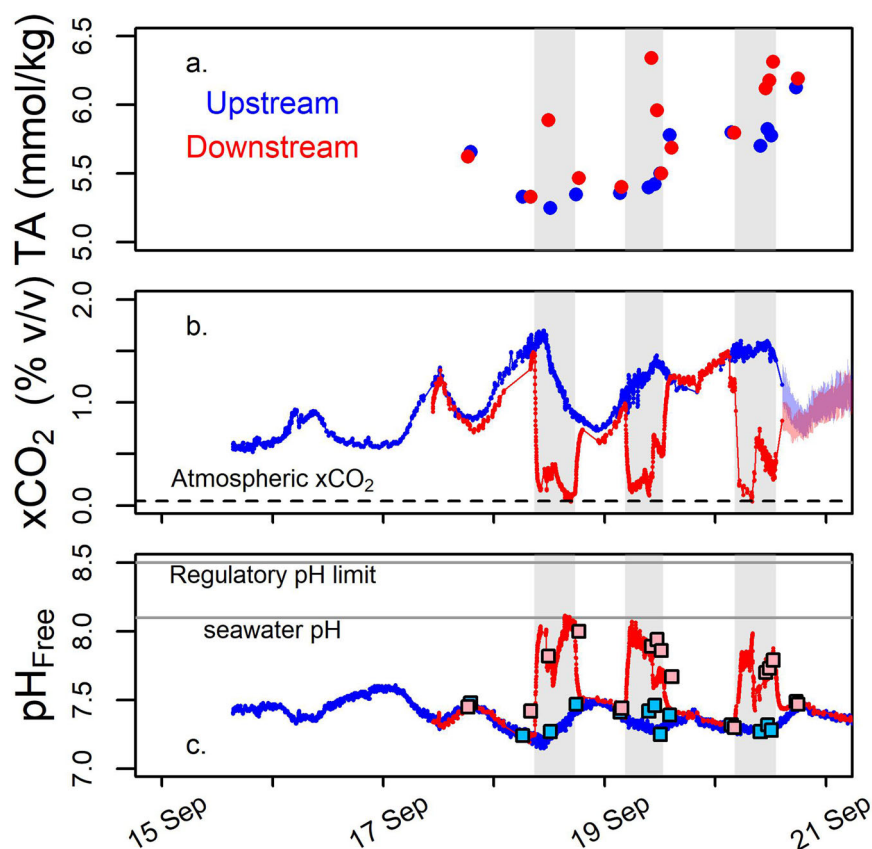
Fig. 1 | Laboratory addition of $\text{Mg}(\text{OH})_2$ to wastewater. Water properties against the fraction of MH suspension in wastewater. TSS was determined immediately (<3 min; light blue in top right panel; TSS_{in}) and 18 h after the addition of MH (dark blue in top right panel; $\text{TSS}_{18\text{h}}$). Dotted lines represent best fit for pH and TSS.

Increasing MH fraction in the MH-wastewater mixture led to a reduction in dissolved CO_2 ($\text{CO}_2(\text{aq})$) and increase in TA from 5.5 mmol/kg up to 8.4 mmol/kg at 1% v/v MH suspension in wastewater (Fig. 1 and supplementary Table S-1). DIC remained unchanged as expected from conservation of mass (CO_2 was converted to HCO_3^- and CO_3^{2-} , but the sum remained the same), suggesting that no precipitation of inorganic carbon took place in these experiments. The pH of the wastewater mixtures increased with increasing MH fraction, in agreement with previous studies for the addition of laboratory grade $\text{Mg}(\text{OH})_2$ and the Mg-rich minerals brucite and olivine to seawater^{13–16}. Thereby, 0.01% and 0.1% MH suspensions in wastewater effected pH increases of 0.2 and 1.2 units respectively. A logarithmic curve was fitted to our experimental pH data: $\text{pH}_{\text{lab-experiments}} = 0.316 \times \ln(\text{MH}_{\% \text{ Volume Fraction}}) + 9.26$. Total suspended solids (TSS), quantified immediately (TSS_{in}) and 18 h after MH addition ($\text{TSS}_{18\text{h}}$), demonstrated dissolution of particulate MH. We assume that $\Delta\text{TSS} = \text{TSS}_{\text{in}} - \text{TSS}_{18\text{h}}$ represented the sum of dissolved $\text{Mg}(\text{OH})_2$ plus that consumed by H_2CO_3 in wastewater. Given a molecular weight of 58.3 g/mol, we calculated the ΔTSS -equivalent [$\text{Mg}(\text{OH})_2$] as 0.5, 3.8, and 14.2 mmol/kg for the 0.01%, 0.1%, and 1% v/v MH additions respectively. Since these estimates exceeded the solubility of $\text{Mg}(\text{OH})_2$ in pure-water (~0.3 mmol/kg), $\text{Mg}(\text{OH})_2$ must be consumed by the abundant H_2CO_3 in wastewater. The conversion of CO_2 to HCO_3^- through this reaction was corroborated by a geochemical speciation model using the concentration of alkalinity, pH, CO_2 partial pressure (pCO_2), temperature, and added Mg as input parameters¹⁷. Finally, there was no evidence of struvite or vivianite precipitation which could cause operational disruption of the HWTW. Phosphate and ammonia data, which decreased conservatively with increasing MH fraction, would have decreased non-conservatively if precipitation had taken place. Our experiments determined a mixing ratio of ~0.02% v/v MH suspension in wastewater for the field trial (equivalent to 104 mg/L or 1.8 mmol/kg $\text{Mg}(\text{OH})_2$ addition).

Following the lab experiments, MH was pumped directly into ‘final effluent’ at the HWTW on three consecutive days (18th–20th September 2022) for ~8.5 h per day at 0.058 L/s into a wastewater flow of 270 ± 70 L/s (\pm standard deviation) giving a mean mixing ratio of $0.021 \pm 0.008\%$ v/v [110 mg/L or 1.9 mmol/kg $\text{Mg}(\text{OH})_2$]. Monitoring stations, upstream and downstream of the addition, were separated by approximately 200 m with a mean residence time of 22 min (MH addition to CO_2 /pH change was 16–33 min). Thereafter, effluent was discharged via an 11.3 km pipeline (residence time of ~9 h) terminating 2.5 km offshore in four diffusers at 23 m depth.

The addition of MH to treated effluent at the HWTW led to a decrease in xCO_2 (the mixing ratio of CO_2 in air-equilibrated-wastewater) and concomitant increase in pH and TA (Fig. 2). Prior to and between MH additions, downstream data were consistent with the upstream data with average xCO_2 of $1.36 \pm 0.20\%$ v/v (range: 0.6–1.5% v/v or 6000–15,000 ppmv), and pH in the 7.2–7.6 range. During MH addition, xCO_2 decreased consistently with average xCO_2 of $0.36 \pm 0.28\%$ and to a minimum of 0.038% (or 380 ppmv $\times \text{CO}_2$), i.e., close to the atmospheric xCO_2 mole fraction (~410 ppmv). pH increased from 7.38 ± 0.09 (upstream) to 7.78 ± 0.17 during MH addition. There was no significant difference in DIC between paired upstream-downstream samples during MH addition [DIC range 5.4–6.5 mmol/kg; mean difference (\pm st.error) = $29 (\pm 27)$ $\mu\text{mol/kg}$], confirming the conservation of mass for DIC between these stations (supplementary Table S-3). In contrast, addition of MH suspension increased TA consistently by up to 943 $\mu\text{mol/kg}$, equivalent to a 17% increase, compared to concurrent measurements upstream (mean upstream TA: 5591 $\mu\text{mol/kg}$; mean TA difference between paired upstream/downstream samples was 560 $\mu\text{mol/kg}$). From the mean change in xCO_2 and CO_2 solubility at 18 °C¹⁸, we calculated a molar CO_2 change of 410 $\mu\text{mol/kg}$. This gave an efficiency of 0.73 mol CO_2 reduction per mol TA increase or 1.47 mol CO_2 per mol MH for the average alkalinity increase

Fig. 2 | Field addition of $\text{Mg}(\text{OH})_2$ to wastewater. a TA, (b) xCO_2 , and (c) pH timeseries observations upstream (blue) and downstream (red) of $\text{Mg}(\text{OH})_2$ addition to wastewater (grey shaded areas). Squares in panel (c) represent discrete samples. Red and blue shading in (b) represent extrapolated xCO_2 values from pH observations in (c).



(560 $\mu\text{mol/kg}$) in agreement with published efficiencies of 0.6–0.8 mol CO_2 per mol TA^{13,15}. TSS loads at the upstream (59 ± 25 mg/L) and downstream stations (66 ± 45 mg/L) were statistically indistinguishable (t test, $p > 0.05$), confirming significant dissolution of the particulate MH added.

Ocean discharge of enhanced alkalinity wastewater

The signal from the addition of MH to effluent at HWTW was expected to arrive at the diffuser ~ 9 h after the start of dosing (supplementary Table S-1). The periods before and when MH was expected to flow at the diffuser are hereafter referred to as ‘pre-MH’ and ‘during-MH’. Lower salinity water (< 35.1) in the vicinity of the outfall had the characteristics of treated effluent from the HWTW: higher xCO_2 , TA, DIC, ammonia and optical backscatter (a measure of particulates), lower pH, and lower oxygen saturation. TA and DIC were elevated around the outfall by ~ 200 $\mu\text{mol/kg}$ and ~ 100 $\mu\text{mol/kg}$ respectively compared with long-term observations in the nearby coastal English Channel¹⁹. A significant correlation between ammonia and salinity was found for marine samples (Pearson $R^2 = 0.68$, $p < 0.001$) with an intercept of 2316 ± 257 $\mu\text{mol/kg}$, comparable with measurements at HWTW (2774 ± 149 $\mu\text{mol/kg}$).

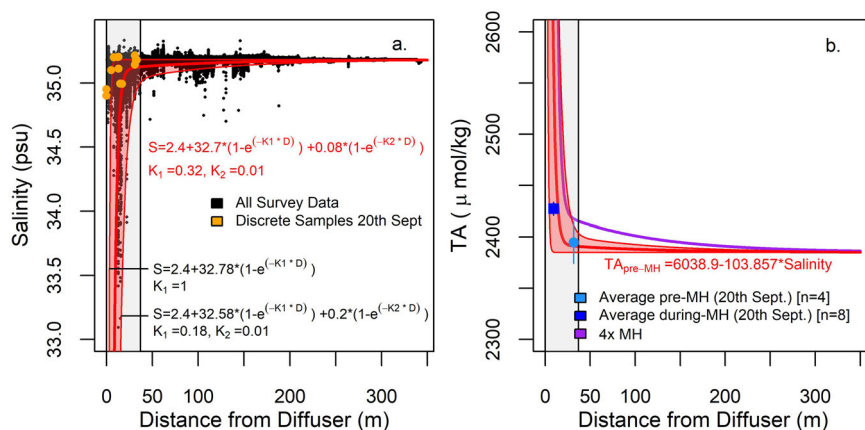
The carbonate system in seawater is constrained by a series of equilibria, such that two of its four variables [TA, DIC, pH, and pCO_2 , the partial pressure of CO_2] can predict the remaining two²⁰. Here, we found agreement between in situ pH or pCO_2 with that predicted from the seawater carbonate equilibrium when DIC was used with pCO_2 or pH as predictors. However, the discrete TA/DIC pair was a poor predictor of pH/ pCO_2 . When the average TA calculated from pCO_2 /DIC was subtracted from the average measured TA, we found an ‘excess alkalinity’ of 55.2 $\mu\text{mol/kg}$ ($\text{TA}_{\text{measured}} > \text{TA}_{\text{calc}}$), likely reflecting the presence of organic alkalinity in wastewater (weak organic bases). While organic alkalinity contributes to TA in the short term, this is likely a transient effect (hours-days) as the remineralisation of organic bases would lead to both CO_2 production and a reduction in TA²¹. This transient contribution of organic alkalinity and its biogeochemical

evolution (dilution, remineralisation) are beyond the scope of this paper, but worthy of further study in the context of OAE.

Diurnal TA variability close to the diffuser (up to 150 $\mu\text{mol/kg}$), was consistent with TA variability at HWTW (Fig. 2), thermal stratification as well as tidal- and wind-driven mixing and advection of seawater. Direct measurement of alkalinity enhancement at the marine discharge was confounded by rapid dilution of the wastewater which is illustrated by the salinity distribution with distance from the diffuser (Fig. 3a.). In order to constrain this mixing, we constructed a mixing model with two end-members: (a) final effluent with salinity 2.4 and (b) coastal seawater with salinity 35.18 (average salinity 300–350 m from diffuser). An exponential fit was used to describe the relationship between salinity and distance from the diffuser [$\text{Salinity} = 2.4 + 32.7 \times (1 - e^{-K_1 \times D}) + 0.08 \times (1 - e^{-K_2 \times D})$], where D is the distance from the diffuser, $K_1 = 0.32 \text{ m}^{-1}$ and $K_2 = 0.01 \text{ m}^{-1}$ are empirical constants which define how rapidly the end-members mix. Salinity observations were broadly constrained by K_1 in the range of 0.18–1.00 m^{-1} and K_2 in the range of 0–0.01 m^{-1} (Fig. 3a.). The salinity mixing curves from this model were used to constrain the extent of the ‘initial mixing zone’ (IMZ), the region where the final effluent rises under its own buoyancy^{22,23}. We defined the edge of the IMZ as salinity = 35 psu. For $K_1 = 0.18 \text{ m}^{-1}$ and $K_2 = 0.01 \text{ m}^{-1}$ (higher mixing scenario), the outer edge of the IMZ was thereby calculated as 38 m (grey shaded area in Fig. 3). The model IMZ salinity was used to calculate the respective fractions of effluent/seawater and an average dilution factor of 260 within the IMZ (590 at the edge of the IMZ).

Final effluent dilution was in agreement with the range of dilution factors from hydrodynamic modelling (400–2700)²⁴, but also suggested that the alkalinity enhancement at HWTW would be practically undetectable in the IMZ. The 260-fold effluent dilution in the IMZ suggested that the alkalization at HWTW (< 943 $\mu\text{mol/kg}$) should be practically undetectable at sea (3.6 $\mu\text{mol/kg}$). A meaningful comparison of pre- and during MH TA could only be done for the 20th of September (logistical constraints on previous days resulted in the collection of a single during-MH sample). A

Fig. 3 | Ocean dilution of Mg(OH)₂ treated wastewater. **a** Salinity against distance from the diffuser (black circles) with discrete samples from the 20th of September (orange circles). Salinity data were fitted with an exponential function (red line and shaded area) which were used to define the ‘initial mixing zone’ (grey shaded area). **b** Mean TA for pre-MH (light blue circle) and during-MH samples (dark blue square) from the 20th of September (error bars are standard deviation). TA_{pre-MH} (red curve) was derived from salinity in (a), and the linear regression of TA against salinity. The red shaded area corresponds to the range of mixing curves in (a). The purple curve represents a four-fold increase in MH addition.



during-MH TA increase of $33.8 \pm 14.7 \mu\text{mol/kg}$ was measured (average during-MH TA = $2415.8 \mu\text{mol/kg}$, compared to $2382.0 \mu\text{mol/kg}$ pre-MH). Closer examination of the data revealed a sampling bias whereby during-MH samples were collected closer to the diffuser compared to earlier samples which would result in higher TA regardless of MH addition. Salinity from the mixing model above was combined with the TA-salinity regression for pre-MH coastal and HWTW upstream discrete samples ($TA_{pre-MH} = 6038.9 - 103.857 \times \text{Salinity}$, $R^2 = 1.00$, $n = 18$, $p < 0.001$), to calculate the corresponding TA with distance from the diffuser (red line in Fig. 3b). Both pre- and during-MH TA on the 20th of September fell within the envelope of the mixing model (Fig. 3b). Similarly, DIC was related to salinity for pre-MH coastal and HWTW upstream discrete samples ($DIC_{pre-MH} = 6535.0 - 125.212 \times \text{Salinity}$, $R^2 = 0.999$, $n = 18$, $p < 0.001$) and the observed during-MH and pre-MH DIC difference ($2154.7 \mu\text{mol kg}^{-1}$ ($n = 8$) and $2122.7 \mu\text{mol kg}^{-1}$ ($n = 4$) respectively) could be ascribed to dilution within the initial mixing zone. We therefore concluded that the observed TA and DIC increase could be ascribed to proximity to the diffuser rather than the addition of MH. These findings confirm the difficulty of measuring small TA changes against a high background at sea.

Nevertheless, we found other carbonate system effects, consistent with alkalization. In the immediate vicinity of the diffuser (within 5 m) and at salinities < 35.1 psu: (a) during-MH $x\text{CO}_2$ was lower by $27.2 \mu\text{atm}$ and (b) pH was higher by 0.017 units compared to earlier observations on the same day (Fig. 4). Both of these parameters were consistent with alkalization of the effluent. Modest CO_2 reduction was thereby corroborated by independent measurements of $x\text{CO}_2$ and pH during this ‘proof of concept’ trial. Our observations demonstrate that $x\text{CO}_2$ and pH are more suitable parameters for OAE monitoring than TA, because of lower background values for $x\text{CO}_2$ and established sensor technologies that allow continuous observations rather than discrete sampling.

Discussion

Alongside deep and rapid cuts in CO_2 emissions, early CDR deployment will be required in order to limit global warming and maintain ocean health²⁵. Here, the addition of MH achieved substantial wastewater alkalinity enhancement and CO_2 reduction with an efficiency of 0.73 mol CO_2 reduction per mol TA added. It is worth noting that downstream recovery to pre-addition conditions was rapid with no apparent ‘memory’ of the MH addition in either the TA, $x\text{CO}_2$ or the pH data. From an operational and regulatory perspective, this demonstrates a clear ‘exit strategy’ should the MH addition need to be stopped. Without addition of MH, the wastewater was supersaturated with respect to atmospheric CO_2 and this excess CO_2 ($34 \times$ atmospheric equilibrium) would therefore be expected to degas to the atmosphere once discharged to the ocean. Post-discharge CO_2 reduction and pH increase, consistent with alkalization, were confirmed, but direct detection of these was limited to within a few metres of the diffuser due to the modest addition of MH, primarily aimed at ‘proof-of-concept’.

The specific location of this trial maximises the CDR potential of alkalization as the prevailing currents would maintain alkalized water in contact with the atmosphere for ~ 4 years²⁶. At the present site, upscaling the MH concentration would lead to complete depletion of the wastewater CO_2 and increase the final effluent pH. A four-fold increase in MH concentration would thereby increase ‘final effluent’ pH to ~ 8.46 (for a 0.08% $\text{MH}_{\% \text{ Volume Fraction}}$). In seawater, our mixing model shows that a four-fold increase in MH addition would raise TA by $19.5 \mu\text{mol/kg}$ at the edge of the IMZ (purple curve in Fig. 3b). The mean area-weighted TA increase within the IMZ would be $49.0 \mu\text{mol/kg}$. We expect such an increase in TA to raise pH by 0.11 units (to 8.20) and lower $p\text{CO}_2$ by $111 \mu\text{atm}$ (based on seacarb 3.3.1²⁷, from $461 \mu\text{atm}$). Using a gas transfer model²⁸ and average wind speed of 4.5 m/s , this $p\text{CO}_2$ reduction would switch the IMZ from a current source of CO_2 (efflux of $2.2 \text{ mmol/m}^2/\text{d}$) to a sink for atmospheric CO_2 (influx of $-3.7 \text{ mmol/m}^2/\text{d}$). Seawater pH would thereby remain within both the regulatory limit of 8.5 and the seasonal envelope for these coastal waters (e.g. pH variability of 0.38 units)¹⁹. Within the IMZ, the mean TSS would increase by $\sim 1.0 \text{ mg/L}$ (260-fold dilution of 254 mg/L undissolved TSS in final effluent). Particulate TA, ejected from the diffuser, would reach the sea surface and behave as quasi-dissolved since the settling velocity (settling drag) is at least one order of magnitude lower than the horizontal velocities (drag) from wind and tides. Our calculations also show that a four-fold increase in seawater alkalinity enhancement would increase the aragonite saturation state (Ω_{Ar}) from 2.4 to 3.0, i.e., below the threshold of 7 where CaCO_3 precipitation has been reported which might render alkalization ineffective for CDR²⁹. We stress that lifecycle embedded and operational emissions exceeded the avoided emissions for the present trial due to its limited scale. However, our ‘proof of concept’ trial justifies further work exploring the efficacy of lower emission Mg(OH)_2 and field trials focused on increasing the scale of operations and resulting CDR. Some operational emissions will increase proportionately with upscaling such as those associated with the additional feedstock required. Others, such as transport, dosing, and monitoring setup, increase by a smaller proportion. These considerations are captured in published Monitoring Reporting and Verification protocols (MRV)^{30,31}. Our simple mixing model illustrates the potential of a distributed network of sites, each with modest MH addition, to provide an effective solution as part of a wider climate change mitigation strategy¹³.

While this study demonstrates the CDR potential of alkalinity enhancement using MH and its potential to counteract ocean acidification, it is imperative to consider potential ecosystem impacts. Previous experimental exposure of the shore crab (*Carcinus maenas*) to alkali identified physiological responses at higher pH increases ($+0.4$ and $+0.7$ pH units)³² than observed here or expected from a four-fold increase in MH concentration. Such pH perturbations in seawater are unrealistic for the purpose of CDR as they could lead to precipitation of CaCO_3 with no CDR benefit²⁹. Average Mg(OH)_2 concentration in the IMZ would increase by 1.7 mg/L for a four-fold increase in MH addition to the final effluent. For

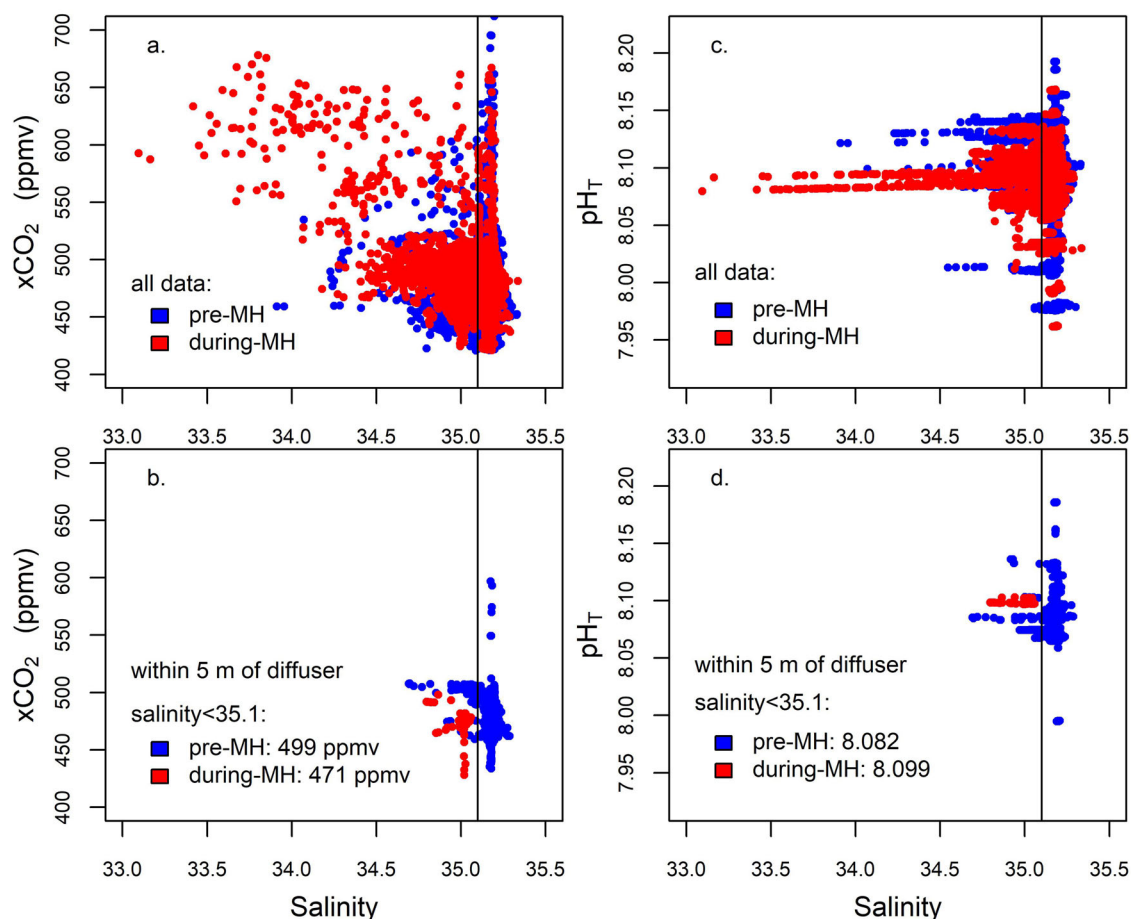


Fig. 4 | Ocean carbonate system properties. **a** $x\text{CO}_2$ against salinity within 350 m and **(b)** 5 m of the discharge of treated wastewater to the coastal ocean. **c** pH against salinity within 350 m and **(d)** 5 m of the discharge. Blue and red symbols denote pre-

MH and during-MH observations respectively. Statistically significant differences were constrained to within 5 m of the discharge point at salinity < 35.1 (vertical line).

reference, $\text{Mg}(\text{OH})_2$ toxicity levels (LC50) for an aquatic invertebrate (*Daphnia magna*) and fish (*Pimephales promelas*) are 285 and 511 mg/L respectively^{33,34} while magnesium ion LC50 is 1300 mg/L and 2100 mg/L respectively³⁵. Based on this evidence, upscaling OAE by addition of $\text{Mg}(\text{OH})_2$ to wastewater can provide a climate change mitigation solution while staying within the range of chemical conditions experienced by marine ecosystems.

Methods

Analytical methods

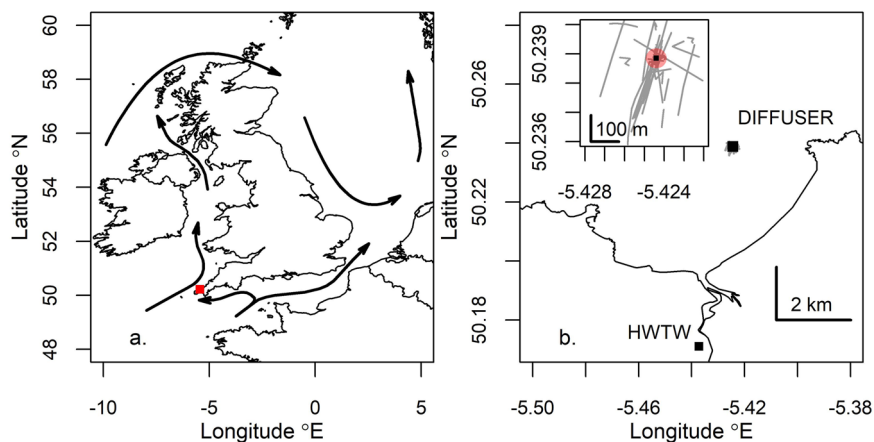
Discrete sample measurements for carbonate parameters were made at 21 ± 0.5 °C from the same subsample in triplicate as described below and in the order of $\text{CO}_2(\text{aq})$, Dissolved Inorganic Carbon (DIC), pH, Total Alkalinity (TA). Sample handling and methodologies followed ‘best practice’ as recommended by Dickson (2007). $\text{CO}_2(\text{aq})$ was determined by sparging a known volume of subsample with N_2 gas (BOC Ltd.) followed by non-dispersive infrared detection of $\text{CO}_2(\text{g})$ (LiCor Biosciences, LI-7000). The LI-7000 instrument was calibrated with acidified Na_2CO_3 standards (see next). DIC was determined by acidifying a known volume of subsample with 8.5% v/v H_3PO_4 , followed by sparging with $\text{N}_2(\text{g})$ and non-dispersive infrared detection (LICOR; LI 7000) using an Apollo SciTech AS-C3 DIC analyser (Kitidis et al., 2017). The instrument was calibrated with Na_2CO_3 standard solutions (range: 0–3.2 mmol/L Na_2CO_3), [prepared by serial dilution of a 0.4 mol/L stock standard solution: 10.599 g of Na_2CO_3 (VWR Chemicals, prod.no. 27767.295; Lot 21C154126), weighed on an ISO9001 calibrated microbalance (Ohaus Explorer Pro, s/n 1127033970) and dissolved in 250 mL of analytical grade water (Millipore, Milli-Q, 18.2 MOhm) which was previously sparged with N_2 gas (BOC Ltd.) in order to remove

background $\text{CO}_2(\text{g})$]. Analytical precision for DIC was < 2 $\mu\text{mol}/\text{kg}$. A certified reference material from the Andrew Dickson laboratory at Scripps Institute of Oceanography (batch # 202) with a reference DIC concentration of 2043.3 $\mu\text{mol}/\text{kg}$ was analysed in triplicate and determined as 2038.1 ± 1.7 $\mu\text{mol}/\text{kg}$.

TA was determined by open cell, dynamic end-point, titration (Dickson, 2007) with 0.0396 mol/L HCl solution (diluted from 10 mol/L HCl, Merck ACS, prod.no. 30721, Lot STBG8596) and calibrated with Na_2CO_3 standard solutions described above using an automated titration system (Metrohm, 916 Ti-Touch, s/n: 1916002032101) with a 20 mL dosing unit (Metrohm 800 Dosino, s/n: 1800003010533) and glass electrode (Metrohm iConnect 854; s/n: 00682610). The certified reference material from the Andrew Dickson laboratory (batch # 202) with a reference TA concentration of 2215.1 $\mu\text{mol}/\text{kg}$ was analysed in triplicate and determined as 2220.7 ± 5.6 $\mu\text{mol}/\text{kg}$.

In the laboratory pH was determined with a glass electrode (Metrohm iConnect 854; s/n: 00682610). The instrument was calibrated with 3 NBS buffers at pH4 (Fisher, prod.no. J/2826/15, Lot 2034055), pH7 (Fisher, J/2855/15, Lot 2028757) and pH10 (VWR Chemicals, prod.no. 85044.001, Lot 211014118). The calibration slope was 99.8% of the idealised Nernst slope. Note that pH is reported on the NBS scale here (pH_{NBS}). Inorganic nutrients samples were collected by filtering 50 mL of effluent into acid cleaned high density polyethylene (HDPE) bottles (Whatman, WHA10404006, 0.45 μm cellulose acetate filter), and then frozen at -20 °C and transported back to the laboratory for analysis. The samples were defrosted according to GO-SHIP nutrient protocols³⁶. Dissolved inorganic nutrient concentrations were determined by colorimetric analytical techniques using a 5-channel Bran and Luebbe segmented-flow autoanalyzer

Fig. 5 | Study area. **a** Study area and location of the MH addition field trial in north Cornwall, UK (red square). The general residual circulation follows the black arrows, flowing North from the study area, clockwise around Great Britain and counter-clockwise around the North Sea. **b** Locations of the Hayle Wastewater Treatment Works (HWTW) where MH suspension was added to final effluent and diffuser at the end of the discharge pipe for final effluent (black square). The inset shows the survey tracks around the diffuser (black square) and extent of the initial mixing zone (red shaded area).



(Bran and Luebbe, model AA3). Standard analytical techniques were used for nitrate + nitrite ($\text{NO}_3^- + \text{NO}_2^-$)³⁷, nitrite (NO_2^-)³⁸, ammonia + ammonium (NH_x)³⁹, phosphate (PO_4^{3-})⁴⁰ and silicate (SiO_2^-)⁴⁰. All sample handling and analysis was carried out according to GO-SHIP nutrient protocols.

Total Suspended Solids (TSS) were determined as dry weight per litre following the regulatory analytical protocol (ISBN 011751957X). A known volume of water was filtered through dry, pre-weighed glass fibre filters (1.2 μm nominal pore size; Whatman, GF/C), dried at 105 °C and reweighed (balance: Ohaus Explorer Pro, s/n 1127033970). The dry retentate was divided by the volume of sample filtered to derive TSS concentration. TSS samples were air-dried in the field (within 12 h of collection) prior to drying at 105 °C overnight at the PML laboratory (1–5 days post-collection).

Lab assessment of alkalinity enhancement in wastewater

Prior to the field trial, laboratory experiments were conducted in order to: (a) assess the impact of MH addition on the wastewater carbonate system, (b) determine field-trial dosing rates within the regulatory discharge framework (upper pH limit of 8.5 and TSS limit of 150 mg/L at the edge of the ‘initial mixing zone’ at sea) and (c) assess the potential formation of struvite ($\text{NH}_4\text{MgPO}_4 \cdot 6\text{H}_2\text{O}$) and vivianite ($\text{Fe}_3(\text{PO}_4)_2$), precipitates that could consume MH and thereby compete with CO_2 as well as cause operational disruption of the wastewater treatment plant (WTW). Wastewater from Hayle WTW (HWTW) was mixed with a commercial MH suspension (TIMAB Magnesium; TIMAB 53 S mare). Circa 990 mL of wastewater were transferred to a 1 L volumetric cylinder before pipetting the corresponding volume of MH suspension and adding more wastewater up to the 1 L mark. The volumetric cylinder was inverted and the solution was gently transferred to 0.5 L glass bottles with a ground neck and stopper. Particular care was taken during the transfer in order to avoid turbulent mixing and bubble formation as well as headspace formation in the incubation bottle.

Field trial setup - Hayle wastewater treatment works

MH suspension (TIMAB magnesium, TIMAB 53 S mare, magnesite) was added to ‘final effluent’ at the Hayle wastewater treatment works (HWTW) on three consecutive days for ca 8.5 h on the 18th, 19th, and 20th of September 2022. The start times, pipe volume, and flow data provided by South West Water Ltd. were used to calculate the expected time of MH arrival at the diffuser outside St. Ives Bay (supplementary Table S-2). MH suspension was supplied in four intermediate bulk containers (IBC), agitated with an industrial IBC mixer (Axesspack, TM IBC-169) and delivered to the effluent at a constant rate of 3.5 L/min using an industrial slurry dosing pump (Verderflex, iDura 15). In total, 4 tonnes of MH suspension were added to the final effluent.

Monitoring stations were established upstream (50.171846°N, 5.434764°W) and downstream (50.171283°N, 5.436859°W) of the MH addition and were instrumented with CO_2 and pH sensors with additional discrete sampling for DIC, TA and pH, nutrients and TSS (Fig. 5). Two

custom-made, autonomous sampling systems were installed at the wastewater treatment works on 15th September 2022. Water was drawn from a sump at the upstream and downstream stations using a custom-made, solar-powered pump system (Blackfish Engineering, Bristol, UK). Each system comprised a diaphragm pump (Flojet, RLFP 222202D), two 400 W solar panels, 440 Ah battery capacity, timer, and associated electronic circuitry. Pumped effluent was directed to a flow-through manifold housing a CO_2 sensor (ProOceanus CO_2 Mini), pH sensor, and logger (Hobo MX2501 pH and Temp). The CO_2 sensors were factory calibrated and the pH sensors were calibrated prior to deployment using NBS buffers. Wastewater flow through the sensor manifold was regulated to 2 L/min (manufacturer recommends 1–3 L/min for the CO_2 Mini). Both pump systems were operated on a timer, switching on/off every 15 min, apart from the MH addition periods when the pumps were operating continuously. The outlet of the flow-through manifold returned wastewater to the sampling sump and was used for discrete sample collection. Both CO_2 Mini sensors unexpectedly stopped on the 20th of September at 14:33 BST (at the end of the last MH addition). Subsequent CO_2 data were inferred from the CO_2 -pH relationship prior to this point ($\text{CO}_2 = 21521997120 \times e^{-3.22\text{pH}}$), propagating a pH uncertainty of 0.05 units (shaded area in Fig. 2). Discrete samples were collected for analysis of carbonate system parameters (DIC, TA, pH), nutrients and TSS following the protocols described above.

Field trial setup - Coastal ocean survey

Sampling at the diffuser outside St. Ives Bay took place on a 20 m long survey vessel and a 7 m long fishing vessel (static vessel) over the period 18–21 September 2022. The static vessel assumed a position at the diffuser site while the survey vessel carried out spatial survey work consisting of a series of stations and drifts (Fig. 5). In calm conditions and slack water during the tidal cycle, the diffuser was identifiable at the surface as four clear patches suggesting four diffusers spaced fifteen metres apart and in line with the known position of the outflow pipe on land. The northernmost diffuser is located at approximately 23 m depth at 50.23885°N, –5.424404°E with the other diffusers on a bearing of 117°. Ship positions were logged from the navigational instruments of both vessels at half-hourly intervals and at the start/end of stations/drifts. These data were interpolated onto the sampling times and their horizontal distance from the northernmost diffuser calculated using the Haversine formula.

The static vessel was equipped with a Conductivity Temperature Depth (CTD; RBR Concerto3, s/n 60614) and CO_2 sensor package (ProOceanus CO_2 -PRO) which was deployed at anchor, primarily centred on the second diffuser from North. A 12 V submersible pump (Seabird) was used to maintain a constant flow across the CO_2 sensor head, powered by a 78 Ah battery pack. Data were logged internally and downloaded daily. The sensor package was deployed at constant depths (either at 17 m or 10 m) for several hours at a time.

The survey vessel was equipped with a multiparameter CTD (RBR Maestro3, s/n 209876) with additional backscatter, dissolved oxygen and pH

sensors (pH was factory calibrated and checked against the same buffers as the lab electrode – no recalibration required). A 28 m flexible hose (10 mm id) was attached to the instrument wire with the inlet co-located with the CTD. This setup was used in ‘profiling’ mode, drawing water from the CTD depth. Water was drawn on deck via a diaphragm pump (Flojet, RLPF 222202D) and directed to a flow-through manifold housing a CO₂ sensor (ProOceanus CO₂-PRO CV), pH sensor (Sunburst Technologies, SAMI-pH, s/n 0002) and conductivity probe (RS Components, RS PRO 205-0958). This setup was chosen to facilitate power independence (the setup was 12 V battery powered) and quasi real-time data monitoring with a hysteresis of 28 s (the residence time of the sampling hose). The CO₂ sensor was factory calibrated and the pH sensor was calibrated using NBS buffers prior to deployment and following the manufacturer’s instructions. The flow through the sensor manifold was regulated to 2 L/min. Discrete samples were collected from the flow-through manifold outflow for analysis of carbonate system parameters (DIC, TA, pH), nutrients, and TSS following the protocols described above (supplementary Table S-4). All instruments were synchronised with the clock of the same PC and GMT to facilitate data merging.

Marine xCO₂ data processing

CTD, CO₂, and pH sensor data were merged giving a combined 2 Hz dataset (CTD logging frequency was 8 Hz which was averaged to 2 Hz, interpolating the 1 s CO₂ data and 1 min SAMI-pH data). A 28 s offset was applied to the survey vessel CO₂ and pH data in order to account for the residence time of the sampling hose. The merged dataset was filtered to exclude: (a) all data where the timestamp difference between the CTD and CO₂-PRO CV exceeded 1 s (this removed instances where either instrument was not operational); (b) all data where the salinity was <33 (spurious singular data points in time against a background of salinity >33); (c) a station on the 19th September when instruments were not operating properly (constant values for all parameters apart from time and depth); (d) all data in the uppermost 20 cm of the water column (mostly data at the start of a profile); (e) all data in the uppermost 1 m of the water column with salinity <34.62 (spurious singular data points in time; similar to b and d).

The filtered merged dataset comprised 97,566 data points from the survey vessel and a further 62,268 from the static vessel.

During deployment, it became apparent that the CTD (and hose inlet) drifted into and out of the outfall plume for short periods (typically seconds to <1 min). These events manifest themselves as salinity excursions (>33 salinity) and further corroborated by elevated backscatter compared to background seawater (ca. 35.2 salinity). It appears likely that the turbulent flow directly above the diffuser diverted the CTD package outside of the effluent plume, inhibiting observations for longer periods. During these salinity excursion events CO₂ increased as expected, but was lagging behind salinity (Fig. 6). Salinity would thereby decrease, but CO₂ would not rise concurrently and often peak after the salinity excursion event (see xCO₂ raw

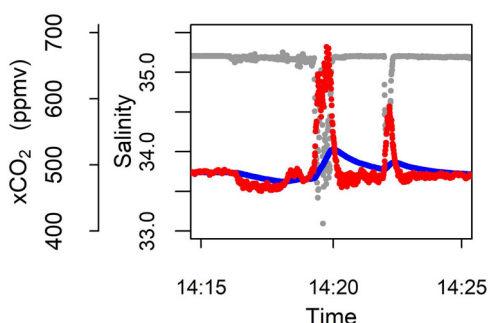


Fig. 6 | Wastewater plume sampling. A salinity excursion event on the 19th of September 2022 showing the time-lag in concurrent CO₂-PRO CV data (xCO₂ raw) and reduced time-lag for scaled data (xCO₂ scaled). Note that the scaling applied here improves the time-lag between low salinity events and xCO₂, although some hysteresis remains.

in Fig. 6). This resulted in a salinity-CO₂ mismatch likely caused by the relatively slow diffusion of CO₂ across the gas-permeable sensor membrane. The diffusion step results in a t63 response time of 50 s (the time it takes for the sensor to reach 63% of full response to a signal). The data were therefore scaled by the 1st and 2nd derivative of CO₂ over 3 s to obtain CO₂ scaled. This calculation improved the matchup between salinity excursion events and concurrent increase in CO₂, but it also amplified the natural ‘noise’ of the CO₂ sensor data (see xCO₂ scaled in Fig. 6). Note that the equation below refers to xCO₂ for technical consistency, where ‘x’ marks the mixing ratio (in ppmv) rather than the partial pressure (in μatm). The scaling equation was empirically optimised to match calculated xCO₂ from discrete TA/DIC samples:

$$xCO_{2\text{ scaled}[n]} = xCO_{2\text{ scaled}[n-2]} + \left(\left(\frac{dxCO_2}{dt} / 3 * 17.26798 \right) + \left(8 * \frac{d^2xCO_2}{dt^2} * 50.79069 \right) \right) / 5 \quad (1)$$

Marine pH data processing

The spectrophotometric instrument reports pH on the total scale at a constant salinity (pH_{SAMI-35}). These data were corrected (pH_{SAMI} in situ) to in situ salinity⁴¹ and further corrected to in situ temperature using the *pHinsi* function in the R-package *seacarb* with the constants of ref. 42, Dickson 1990⁴³, Perez and Fraga, 1987⁴⁴ and Upströhm 1974⁴⁵ (R-version 4.0.1; <https://www.r-project.org/>). Both pH_{SAMI} in situ and measurements using the glass electrode on the RBR instrument (pH_{RBR}) were converted to the free scale using the *pHconv* function in the R-package *seacarb*.

Marine carbonate system quality control and internal consistency

pH_{SAMI} in situ was significantly correlated with measurements using the glass electrode on the RBR instrument (pH_{RBR}) with a residual standard error of 0.008 units (Pearson R² = 1.00, p < 0.001) (Fig. 7). We used the timestamp of discrete samples to find the nearest corresponding pH_{RBR} and pH_{SAMI} in situ. pH_{RBR} was in agreement with pH_{calc} (pCO₂/DIC); calculated pH from the discrete DIC data and corresponding CO₂ partial pressure (pCO₂; calculated from xCO₂ using the *x2pCO2* function in the R-package *seacarb*) (Fig. 7). This agreement between independent instruments gives high confidence to the pH data as well as xCO₂ and DIC data. However, pH calculated from discrete TA/DIC (pH_{calc} (TA/DIC); calculated using the *carb* function in the R-package *seacarb*) did not agree with pH_{RBR}, pH_{SAMI} in situ or pH_{calc} (pCO₂/DIC) (Fig. 7). pCO₂ from DIC/pH was in agreement with measurements of pCO₂ with a standard error of 10.5 μatm (Pearson R² = 1.00, p < 0.001) (Fig. 7). When the average TA calculated from pCO₂/DIC was subtracted from the average measured TA, we found an ‘excess alkalinity’ of 55.2 μmol/kg (55.6 μmol/kg when TA is calculated from DIC/pH).

Final effluent – seawater dilution

Salinity in the vicinity of the diffuser (e.g., within 25 m) was highly variable (range: 33.1–35.3) reflecting extensive and dynamic mixing between final effluent and coastal seawater (Fig. 3a). In contrast, salinity in the zone 300–350 m away from the diffuser was higher on average and much less variable with a mean ± standard deviation of 35.183 ± 0.005 psu (Fig. 3a). We defined two end-member mixing between: (a) final effluent with salinity 2.4 and (b) coastal seawater with salinity 35.183. An exponential fit (Eq. 2) was used to describe the relationship between salinity (S) and distance (D) from the diffuser (red curve in Fig. 3a):

$$S = 2.4 + (32.7) \times (1 - e^{(-K_1 \times D)}) + 0.08 \times (1 - e^{(-K_2 \times D)}) \quad (2)$$

where K₁ and K₂ are empirical constants which define how rapidly the end-members mix. High- and low-mixing variants of Eq. 2 were used to constrain the field-observations (red shaded area in Fig. 3). The mixing

Fig. 7 | Carbonate system internal consistency. **a** pH from the SAMI instrument and calculated from pCO₂/DIC and TA/DIC against pH from the RBR instrument. **b** Measured pCO₂ against calculated pCO₂ from TA/pH.

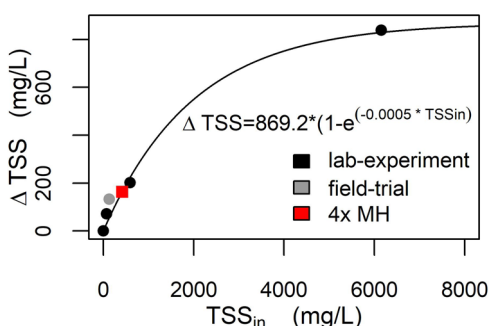
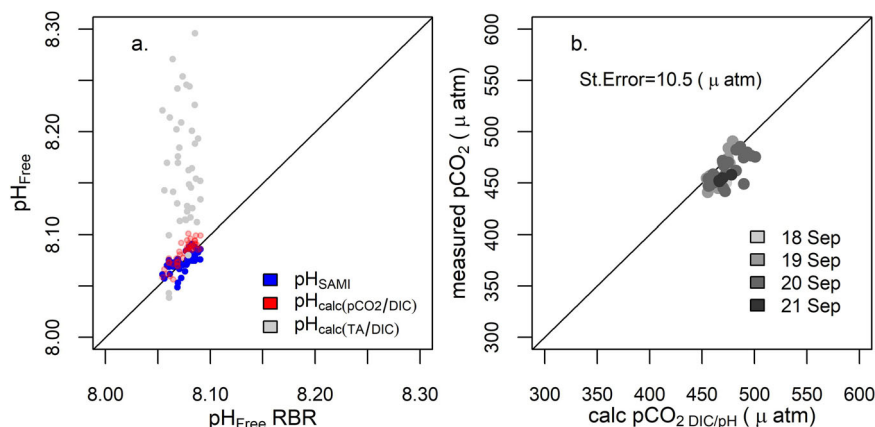


Fig. 8 | Dissolution of solid alkalinity. Dissolution of Total Suspended Solids (Δ TSS) against initial TSS (TSS_{in}) from lab- and field trial data. An exponential asymptotic curve was fitted to the lab-experiment data (solid curve). The red square represents a hypothetical four-fold upscaling of MH addition from the field trial (to 0.08% v/v MH suspension in wastewater).

curves defined by K_1 and K_2 where used to constrain the extent of the ‘initial mixing zone’ by specifying a salinity of 35.00 psu at its outer edge under the low mixing scenario (i.e., within 0.18 psu of the seawater end-member). The outer edge of the initial mixing zone was thereby calculated as 38 m (grey shaded area in Fig. 3).

In order to calculate the dilution of final effluent by coastal seawater, we defined two end-members: (a) final effluent with salinity 2.4 and (b) coastal seawater with salinity 35.183. For any sample point, its salinity is given by Eq. 3:

$$\text{Salinity} = \text{Salinity}_{FE} \times f_{FE} + \text{Salinity}_{sea} \times f_{sea} \quad (3)$$

where Salinity_{FE} and Salinity_{sea} are the respective salinities of the final effluent (2.4 psu) and coastal seawater (35.18 psu). f_{FE} and f_{sea} are the fraction of final effluent fraction of seawater with which it mixes. Since the salinities of the samples and end-members were known, we solved Eq. 2 for f_{FE} given that $f_{FE} + f_{sea} = 1$. The final effluent dilution factor (DF) is then given by Eq. 4:

$$DF = \frac{f_{sea}}{f_{FE}} \quad (4)$$

The average dilution factor and the respective value at the edge of the initial mixing zone were calculated as 260 and 590.

At the point of discharge, the flow velocity would dissipate rapidly. Assuming that the 0.270 m³/s flow is divided equally between the four diffusers, each with a diameter of 60 cm, we calculate a mean upwards velocity of 24 cm/s from each diffuser. If we assume that this velocity dissipates with increasing volume in the IMZ cone, then the effluent would require ~3 min to reach the surface.

As an independent coherence test we calculated the mean current in the initial mixing zone. f_{FE} and f_{sea} can be replaced by the final effluent flow (0.270 m³/s) and a theoretical seawater flow, Flow_{sea} (units: m³/s) in Eq. 3. Flow_{sea} can then be calculated iteratively by varying Flow_{sea} to minimise the absolute difference between measured and calculated salinity using Eq. 3 (replacing f_{FE} with a flow of 0.270 m³/s while f_{sea} becomes Flow_{sea}). We assumed that Flow_{sea} is flowing across the wastewater plume represented as the orthographic projection of a cone on the vertical water column plane, i.e., an inverted triangle with its apex at the diffuser, a height of 23 m (the water depth at the diffuser), spreading to a width (base of the triangle) of 2×38 m at the surface (plume-plane area $A = (23 \times (2 \times 38))/2$ m²). The mean current is thereby calculated as Flow_{sea} divided by the plume-plane area (units: m³/s divided by m² = m/s). This calculation gave a mean current of 0.16 knots which is within the 0.1–0.4 knots neap-tide currents for the area⁴⁶.

Magnesium hydroxide dissolution and upscaling

The lab experiment and field trial TSS data showed complete dissolution of MH at volumetric mixing ratios up to 0.021% v/v MH in wastewater. For, the 0.1% and 1% v/v ratios in the lab experiment, the respective TSS_{18h} concentrations, i.e., undissolved MH, were 390 and 5314 mg/L above the background TSS in raw effluent (supplementary Table S-1). In order to quantify TSS dissolution we fitted an exponential asymptotic curve to the lab-experiment data: $\Delta TSS = 869.2 \times (1 - e^{(0.0005 \times TSS_{in})})$, where $\Delta TSS = TSS_{in} - TSS_{18h}$ (Fig. 8). ΔTSS was assumed to represent dissolved MH.

The TSS dissolution fit above, was used to calculate dissolved and particulate MH loads under a hypothetical four-fold increase in MH dosing to 0.08% v/v MH addition to wastewater. Under this scenario, the concentration of TSS_{in} at the point of MH addition would be 418 mg/L 53% solids/L MH of which 98.5% is Mg(OH)₂ = 522 g/L Mg(OH)₂ in the pure MH suspension applied as 0.08/100 to wastewater = 418 mg/L Mg(OH)₂. Of the 418 mg/L TSS_{in} , our ΔTSS fit predicts dissolution of 164 mg/L, leaving 254 mg/L of undissolved TSS in the final effluent. Given a dilution factor of 260 for the final effluent in the IMZ, we would expect the mean IMZ TSS to be ~1.0 mg/L higher. Assuming that the 164 mg/L dissolved TSS represents MH, we calculate an increase of 2.8 mmol/kg Mg(OH)₂ or 5.6 mmol/kg TA (164 mg/L ÷ 58.3 g/mol and 1 mmol Mg(OH)₂ = 2 mmol TA). The 254 mg/L of undissolved TSS equates to 4.4 mmol/kg Mg(OH)₂ or 8.7 mmol/kg particulate TA. The total (dissolved+ particulate) TA increase in final effluent would thereby be 14.3 mmol/kg.

The dilution of a 14.3 mmol/kg TA addition in coastal seawater is shown as the purple curve in Fig. 3b. This mixing curve, implicitly assumes that the TA addition is in the dissolved or quasi-dissolved phase which is further discussed below. In the initial mixing zone, we would therefore expect a mean TA increase of 55 µmol/kg (260-fold dilution). The 14.3 mmol/kg MH addition to wastewater equals 418 mg/L Mg(OH)₂, or 152 mg/L Mg²⁺. Within the IMZ, we would therefore expect average Mg²⁺ to increase by 0.6 mg/L. In order to examine the behaviour of the

undissolved MH, we used Stokes Law to calculate the settling velocity (w) of a typical MH particle:

$$w = \frac{2(\rho_p - \rho_f)gr^2}{9\mu} \quad (5)$$

where ρ_p and ρ_f are the density of the particle (2300 kg/m³) and fluid (1000.3 kg/m³ for wastewater; 1025.8 kg/m³ for seawater), g is the acceleration of gravity (9.81 m/s²), r is the particle radius (1 μ m) and μ is the dynamic viscosity of the fluid (0.001 kg/m*s). The settling velocity of a particle was thereby calculated as 1.0 cm/h in both wastewater and seawater. Within the 1 m diameter pipe, the mean flow of 0.270 m³/s, gives a horizontal velocity of 1.2 km/h. The horizontal velocity is therefore >10⁵ times greater than the settling velocity. Since the drag force is proportional to the flow velocity, the horizontal drag force is more than 100 thousand times greater than the settling drag force. It is therefore highly unlikely that particles would settle in the pipework from HWTW to the coastal ocean.

At the point of discharge, the flow velocity would dissipate rapidly. Assuming that the 0.270 m³/s flow is divided equally between the four diffusers, each with a diameter of 60 cm, we calculate a mean upwards velocity of 24 cm/s from each diffuser. If we assume that this velocity dissipates with increasing volume in the IMZ cone, then the upwards velocity within 1 cm of the surface is in excess of the settling velocity, i.e., particles ejected from the diffuser would reach the sea surface. In seawater, these particles would then take 96 days to settle to the sea floor assuming no further turbulence (23 m divided by 1 cm/h). The MH particles would therefore reach the surface and sink, but at the same time dissolve and convert carbonic acid, from dissolved CO₂, to bicarbonate ions. The reduction in seawater dissolved CO₂ (carbonic acid) would then favour influx of CO₂ from the atmosphere. Tidal currents in this region are in the range of 5–20 cm/h⁴⁶, i.e., the horizontal drag on particles is one order of magnitude greater than the settling drag force. Tidal and wind-driven turbulence in this dynamic shelf-sea environment would therefore likely resuspend particulate TA rather than allow it to settle on the seafloor. This supports the underlying assumption in our mixing model that particulate TA (MH) would practically behave in a quasi-dissolved manner under hypothetical four-fold upscaling (purple curve in Fig. 3b).

Data availability

All discrete sample data are available in the Supplementary tables. Sensor and profile data are available at <https://doi.org/10.6084/m9.figshare.26049460>.

Received: 2 September 2023; Accepted: 10 June 2024;

Published online: 28 June 2024

References

- IPCC. Summary for Policymakers. In *Global Warming of 1.5 °C: IPCC Special Report on Impacts of Global Warming of 1.5 °C above Pre-industrial Levels in Context of Strengthening Response to Climate Change, Sustainable Development, and Efforts to Eradicate Poverty*. 1–24 (Cambridge University Press, Cambridge, 2022). <https://doi.org/10.1017/9781009157940.001>.
- Buck, H. J., Carton, W., Lund, J. F. & Markusson, N. Why residual emissions matter right now. *Nat. Clim. Change* **13**, 351–358 (2023).
- National Academies of Sciences Engineering and Medicine. *A Research Strategy for Ocean-based Carbon Dioxide Removal and Sequestration*. (The National Academies Press, 2022).
- Friedlingstein, P. et al. Global Carbon Budget 2020. *Earth Syst. Sci. Data* **12**, 3269–3340 (2020).
- Revelle, R. & Suess, H. E. Carbon dioxide exchange between atmosphere and ocean and the question of an increase of atmospheric CO₂ during the past decades. *Tellus* **9**, 18–27 (1957).
- National Academies of Sciences, E., and Medicine. *A Research Strategy for Ocean-based Carbon Dioxide Removal and Sequestration*. (The National Academies Press., 2022).
- Rau, G. H. & Caldeira, K. Enhanced carbonate dissolution: a means of sequestering waste CO₂ as ocean bicarbonate. *Energy Convers. Manag.* **40**, 1803–1813 (1999).
- Rau, G. H., Willauer, H. D. & Ren, Z. J. The global potential for converting renewable electricity to negative-CO₂-emissions hydrogen. *Nat. Clim. Change* **8**, 621 (2018).
- Cai, W. J. & Jiao, N. Z. Wastewater alkalinity addition as a novel approach for ocean negative carbon emissions. *Innov.-Amst.* **3**, <https://doi.org/10.1016/j.xinn.2022.100272> (2022).
- Ilyina, T., Wolf-Gladrow, D., Munhoven, G. & Heinze, C. Assessing the potential of calcium-based artificial ocean alkalization to mitigate rising atmospheric CO₂ and ocean acidification. *Geophys. Res. Lett.* **40**, 5909–5914 (2013).
- Butenschön, M., Lovato, T., Masina, S., Caserini, S. & Grosso, M. Alkalization scenarios in the mediterranean sea for efficient removal of atmospheric co2 and the mitigation of ocean acidification. *Front. Clim.* **3**, <https://doi.org/10.3389/fclim.2021.614537> (2021).
- Wang, H. et al. Simulated impact of ocean alkalinity enhancement on atmospheric CO₂ removal in the bering sea. *Earth's Future* **11**, e2022EF002816 (2023).
- He, J. & Tyka, M. D. Limits and CO₂ equilibration of near-coast alkalinity enhancement. *Biogeosciences* **20**, 27–43 (2023).
- Hartmann, J. et al. Stability of alkalinity in ocean alkalinity enhancement (OAE) approaches – consequences for durability of CO₂ storage. *Biogeosciences* **20**, 781–802 (2023).
- Yang, B., Leonard, J. & Langdon, C. Seawater alkalinity enhancement with magnesium hydroxide and its implication for carbon dioxide removal. *Mar. Chem.* **253**, 104251 (2023).
- Montserrat, F. et al. Olivine dissolution in seawater: implications for CO₂ sequestration through enhanced weathering in coastal environments. *Environ. Sci. Technol.* **51**, 3960–3972 (2017).
- Parkhurst, D. L. & Appelo, C. A. J. Description of input and examples for PHREEQC version 3—A computer program for speciation, batch-reaction, one-dimensional transport, and inverse geochemical calculations. 497 (U.S. Geological Survey, 2013).
- Weiss, R. F. Carbon dioxide in water and seawater: the solubility of a non-ideal gas. *Mar. Chem.* **2**, 203–215 (1974).
- Kitidis, V. et al. Seasonal dynamics of the carbonate system in the Western English Channel. *Cont. Shelf Res.* **42**, 30–40 (2012).
- Lewis, E. & Wallace, D. W. R. Program developed for CO₂ system calculations., ORNL/CDIAC-105. (Carbon Dioxide Information Analysis Center, Oak Ridge National Laboratory, U.S. Department of Energy, Oak Ridge, Tennessee, 1998).
- Wolf-Gladrow, D. A., Zeebe, R. E., Klaas, C., Koertzing, A. & Dickson, A. G. Total alkalinity: the explicit conservative expression and its application to biogeochemical processes. *Mar. Chem.* **106**, 287–300 (2007).
- UKgovernment. (1991) Water Resources Act. <https://www.legislation.gov.uk/ukpga/1991/57/contents> (accessed: 28 June 2023).
- UKgovernment. (2020) European Union (Withdrawal) Act (Retained Directive 2008/105/EC). <https://www.legislation.gov.uk/eudr/2008/105/contents> (accessed: 28 June 2023).
- PlanetaryHydrogen. Westward OH₂ GGR Project – Phase 1 Final Report; BEIS Contract - PLA202081. 42 (Planetary Hydrogen, https://assets.publishing.service.gov.uk/government/uploads/system/uploads/attachment_data/file/1075306/planetary-hydrogen-phase-1-report.pdf (accessed: 28 June 2023), 2022).
- Hofmann, M., Mathesius, S., Kriegl, E., Vuuren, D. P. V. & Schellnhuber, H. J. Strong time dependence of ocean acidification mitigation by atmospheric carbon dioxide removal. *Nat. Commun.* **10**, 5592 (2019).

26. Blaas, M., Kerkhoven, D. & de Swart, H. E. Large-scale circulation and flushing characteristics of the North Sea under various climate forcings. *Clim. Res.* **18**, 47–54 (2001).
27. Gattuso J.-P., Lavigne, E. J.-M. H., Orr J. <http://CRAN.R-project.org/package=seacarb> (2021).
28. Nightingale, P. D. et al. In situ evaluation of air-sea gas exchange parameterizations using novel conservative and volatile tracers. *Global Biogeochem. Cy* **14**, 373–387 (2000).
29. Moras, C. A., Bach, L. T., Cyronak, T., Joannes-Boyau, R. & Schulz, K. G. Ocean alkalinity enhancement - avoiding runaway CaCO₃ precipitation during quick and hydrated lime dissolution. *Biogeosciences* **19**, 3537–3557 (2022).
30. PlanetaryTechnologies. *Measurement, Reporting, and Verification (MRV) Protocol for OAE mCDR by mineral addition (V3.0)*, <https://www.planetarytech.com/science/planetarys-oe/planetarys-mrv/> (2023).
31. Gill, S. et al. *Ocean Alkalinity Enhancement from Coastal Outfalls v1.0*, <https://registry.isometric.com/protocol/ocean-alkalinity-enhancement> (2024).
32. Cripps, G., Widdicombe, S., Spicer, J. I. & Findlay, H. S. Biological impacts of enhanced alkalinity in *Carcinus maenas*. *Mar. Pollut. Bull.* **71**, 190–198 (2013).
33. Okamoto, A., Yamamuro, M. & Tatarazako, N. Acute toxicity of 50 metals to *Daphnia magna*. *J. Appl. Toxicol.* **35**, 824–830 (2015).
34. ECHA. *Reaction mass of Magnesium peroxide and magnesium carbonate and magnesium hydroxide and magnesium oxide*, <https://echa.europa.eu/registration-dossier/-/registered-dossier/7087/6/2/2> (2023).
35. ECHA. *Magnesium hydroxide*, <https://echa.europa.eu/registration-dossier/-/registered-dossier/16073/6/2/2> (2023).
36. Becker, S. et al. GO-SHIP repeat hydrography nutrient manual: the precise and accurate determination of dissolved inorganic nutrients in seawater, using continuous flow analysis methods. *Front. Mar. Sci.* **7**, 1–15 (2020).
37. Brewer, P. G. & Riley, J. P. The automatic determination of nitrate in sea water. *Deep-Sea Res.* **12**, 765–772 (1965).
38. Grasshoff, K. in *Methods of Seawater Analysis* (eds K. Grasshoff, M. Ehrhardt, & K. Kremling) 139–142 (Verlag Chemie, 1983).
39. Mantoura, R. F. C. & Woodward, E. M. S. Optimization of the indophenol blue method for the automated determination of ammonia in estuarine waters. *Estuar Coast Shelf S* **17**, 219–224 (1983).
40. Kirkwood, D. S. Simultaneous determination of selected nutrients in seawater. (International Council for the Exploration of the Sea (ICES), Annual Report, 1989).
41. Clayton, T. D. & Byrne, R. H. Spectrophotometric seawater pH measurements - total hydrogen-ion concentration scale calibration of m-cresol purple and at-sea results. *Deep-Sea Res. Part I-Oceanogr. Res. Papers* **40**, 2115–2129 (1993).
42. Lueker, T. J., Dickson, A. G. & Keeling, C. D. Ocean pCO₂ calculated from dissolved inorganic carbon, alkalinity, and equations for K-1 and K-2: validation based on laboratory measurements of CO₂ in gas and seawater at equilibrium. *Mar. Chem.* **70**, 105–119 (2000).
43. Dickson, A. G. Standard potential of the reaction -AgCl(s)+1/2H₂(g)=Ag(s)+HCl(aq) and the standard acidity constant of the ion HSO₄⁻ in synthetic sea-water from 273.15-K to 318.15-K. *J. Chem. Thermodyn.* **22**, 113–127 (1990).
44. Perez, F. F. & Fraga, F. Association constant of fluoride and hydrogen ions in seawater. *Mar. Chem.* **21**, 161–168 (1987).
45. Uppström, L. R. The boron/chlorinity ratio of deep-sea water from the Pacific Ocean. *Deep-Sea Res. Oceanogr. Abstr.* **21**, 161–162 (1974).
46. King, E. V. et al. The impact of waves and tides on residual sand transport on a sediment-poor, energetic, and macrotidal continental shelf. *J. Geophys. Res.* **124**, 4974–5002 (2019).

Acknowledgements

The authors disclose support for the research of this work from the UK Department of Business Energy and Industrial Strategy [Contract PLA202081]. This synthesis was supported by UK NERC funding (CLASS Theme1.2, NE/R015953/1).

Author contributions

Authors V.K., S.A.R., W.J.B., G.H.R., S.F., G.T., and T.F. contributed to the study design, data synthesis, and interpretation. V.K., W.J.B., S.F., M.T., and G.T. contributed to fieldwork. V.K., S.F., M.T., G.T., E.M.S.W., and C.H. contributed to analytical work.

Competing interests

The authors declare that Planetary Technologies (authors S.A.R., W.J.B., G.H.R.) are developing commercial ocean CDR technologies. PML Applications (V.K., S.F., M.T., G.T., E.M.S.W., C.H., T.F.) provided independent and impartial scientific consultancy services to Planetary Technologies as the commercial subsidiary of Plymouth Marine Laboratory (PML).

Additional information

Supplementary information The online version contains supplementary material available at <https://doi.org/10.1038/s43247-024-01506-4>.

Correspondence and requests for materials should be addressed to Vassilis Kitidis.

Peer review information *Communications Earth & Environment* thanks the anonymous reviewers for their contribution to the peer review of this work. Primary Handling Editors: Olivier Sulpis and Joe Aslin. A peer review file is available.

Reprints and permissions information is available at <http://www.nature.com/reprints>

Publisher's note Springer Nature remains neutral with regard to jurisdictional claims in published maps and institutional affiliations.

Open Access This article is licensed under a Creative Commons Attribution 4.0 International License, which permits use, sharing, adaptation, distribution and reproduction in any medium or format, as long as you give appropriate credit to the original author(s) and the source, provide a link to the Creative Commons licence, and indicate if changes were made. The images or other third party material in this article are included in the article's Creative Commons licence, unless indicated otherwise in a credit line to the material. If material is not included in the article's Creative Commons licence and your intended use is not permitted by statutory regulation or exceeds the permitted use, you will need to obtain permission directly from the copyright holder. To view a copy of this licence, visit <http://creativecommons.org/licenses/by/4.0/>.

© The Author(s) 2024